

# EVALUATION OF HELICOPTER INTAKES IN THE PRESENCE OF A ROTOR

R. Heise<sup>1</sup>, C.J. Meyer<sup>2</sup>, T.W. von Backström<sup>3</sup>

<sup>1</sup>Department of Mechanical Engineering, University of Stellenbosch  
Private Bag X1, Matieland, 7602, South Africa  
e-mail: rheise@sun.ac.za

<sup>2</sup>Department of Mechanical Engineering, University of Cape Town  
Private Bag, Rondebosch, 7701, South Africa  
e-mail: cmeyer@ebe.uct.ac.za

<sup>3</sup>Department of Mechanical Engineering, University of Stellenbosch  
Private Bag X1, Matieland, 7602, South Africa  
e-mail: twvb@sun.ac.za

**Keywords:** Helicopter air intake, Rotor flow patterns, Actuator Disk

**Abstract:** A comparison of the performance of top and side opening air intakes on helicopters is presented. The specific focus here is to establish design criteria for the design of fan intakes for tail-rotor-less helicopters, similar to the NOTAR concept, which are characterised by the use of a relatively large fan and associated intake structures. The results are however also applicable to the design of general helicopter engine intakes. CFD studies were done on a generic helicopter fuselage configuration based on the ROBIN body. An actuator disk simulated the main rotor, with the rotor hub also modelled as an actuator disk. Here it is shown how the inclusion of a rotor hub changes the flow field and affects the performance of the intakes. The performance of the top and side intakes is investigated over a range of advance ratios, as well as the effect of the contraction ratio has on the distortion and pressure losses of the intake. No distinct advantage of either the top or side opening intakes could be established. The rotor hub wake was noted as having a strong influence on the intakes, albeit at different advance ratios for the two configurations. Increasing contractions ratios are shown to have a positive effect, though contraction ratios above 3.0 did not show any significant performance improvements

## 1 NONMENCLATURE

$C_D$	Drag coefficient	<b>Subscripts</b>	
$C_L$	Lift coefficient	C	Capture plane
$C_P$	Pressure coefficient	MR	Main rotor
$C_T$	Thrust coefficient	f	Fan face
CR	Intake contraction ratio	<b>Greek</b>	
P	Total pressure [Pa]	$\eta$	Intake efficiency
q	Dynamic pressure [Pa]	$\mu$	Advance ratio
R	Rotor diameter [m]	$\theta$	Sector angle
V	Velocity [m/s]		

## 2 INTRODUCTION

The intake configurations examined here are specifically for use on the internal fan that is required on helicopters making use of a circulation controlled tail boom for torque control. Examples of these tail booms are the NOTAR system that has found some application as well as the experimental CIRSTEL system. A fan is required by both systems to supply air to drive the circulation control slots and the additional tail thruster. This fan is large in comparison to the size of the engine compressor face, and thus the intake assembly becomes a significant component of the airframe structure. This can limit the position for the intake opening as well as the contraction ratio used for the intake, and the current investigations addresses this issue by looking at the aspects that need to be considered when defining the layout of such intakes.

A complication in the design of helicopter intakes is the variable flow environment the intakes have to work in as the helicopter increases its advance ratio. Dominating here is the flow structure of the main rotor, with secondary influences occurring due to the flow around the fuselage.

Two different intake concepts were selected for investigation, one being an intake opening to the top of the fuselage, behind the rotor hub, and the alternative being a sideways opening intake. To investigate the two different intake concepts, CFD studies were done on a generic helicopter fuselage configuration that included an actuator disk to represent the main rotor.

## 3 FUSELAGE AND INTAKE DEFINITION

A generic fuselage configuration was used for the investigation of the intake concepts. This fuselage was based on the ROBIN configuration (Mineck et al<sup>(1)</sup>), modified here to be representative of a tail-rotor-less helicopter fuselage, with a constant diameter tail boom of diameter 0.13R for the circulation control section and an identical main fuselage for both versions. The cowlings were modified to be representative of a single- and twin-engine helicopter, used for the side and top opening intake concepts respectively. The single engine version, used for the side opening intake configuration, had the gearbox cowling extended from the original configuration. The twin on the other hand had the gearbox cowling shortened, with an additional cowling added to form the engine bay cowling. Both fuselages have an 11m rotor diameter to present the helicopters in the light utility class.

Three contraction ratios were investigated for both fan intake versions, namely contraction ratios of 2.5, 3.0 and 3.5. The inlet opening/capture area ( $A_c$ ) was varied to obtain the specified contraction ratios. At 30% of the intake duct length, the duct cross section was also defined. Here the area was defined as being 1.5 times the fan area, and remained constant for the different contraction ratios used. The dimensions of the inlet capture area were scaled linearly to obtain the required contraction ratio.

### Side Intakes

In the general layout of a single engine helicopter the engine is mounted above the fuselage to the rear of the rotor gearbox. Thus the intakes have to open to the side for this configuration, as the fan will be positioned below the engine at the base of the tail boom. Inherently the side intakes form a complicated duct, as the incoming flow has to turn towards the intake, turn inwards to enter the duct and then rearwards again toward the fan face.

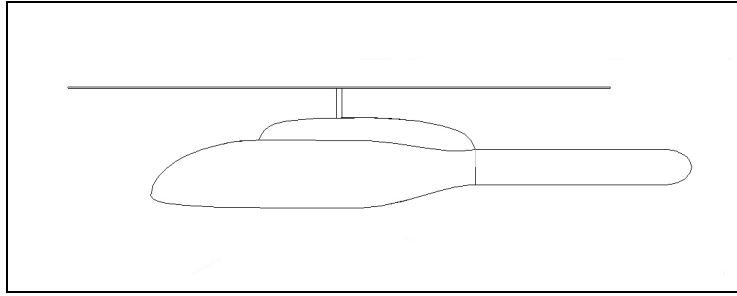


Figure 1 Single engine configuration

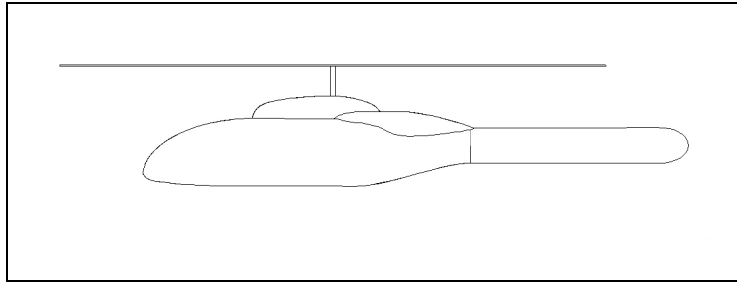


Figure 2 Twin engine configuration

The intakes feature thick lips on the upper rear corner of the inlet opening and a smooth transition of the cowling surface into the intake duct. Also a scoop is included at the bottom of the intake. The capture area of the intake is a 3D curved surface, thus the duct entry is also a complex, blended 3D surface as can be seen in Figure 3.

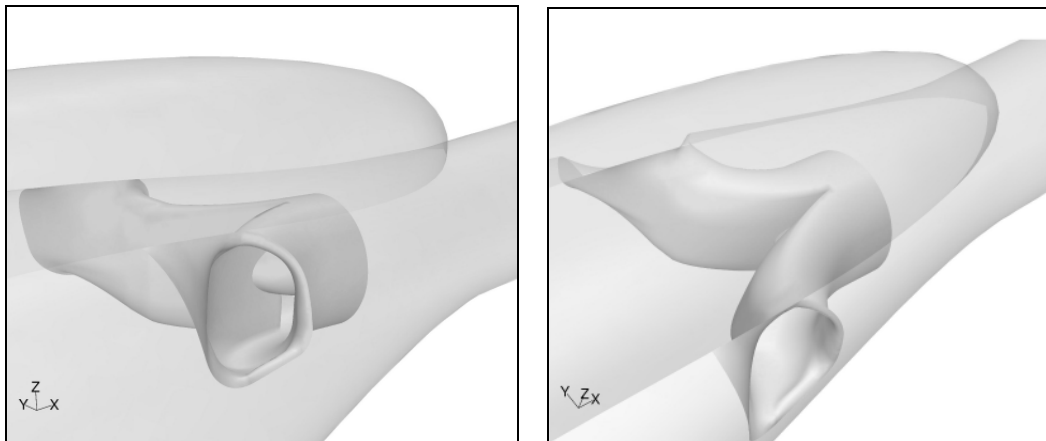


Figure 3 Side intake duct (fuselage displayed semi-transparent)

Design features of the intake include the following:

- Entry area faces slightly upwards, to capture downdraft.
- Scoop included at the lower side of the intake opening to aid in capturing air
- Elliptical intake lips at the rear and bottom sides of the intake

- Duct entry is facing  $57^\circ$  sideways from forward to allow efficient capture at intermediate flight speeds. Duct then turns axially to guide the air into the fan.
- Fan axis tilted upwards by  $7.0^\circ$ .
- Duct cross section changes from rectangular at capture area to double-elliptical to semi-circular, before joining up with the opposing side duct ahead of the fan. Due to the short duct length no effective Gerlach shaping (described by Seddon et al<sup>(2)</sup>) could be implemented, as this would cause a too distorted duct shape. The double-elliptical section at the duct bend is however elongated for better flow turning, as described by Sawyer<sup>(3)</sup>.

### Top Intake

The top mounted intake is designed for the twin engine helicopter for fitment between the two engines. For the top intake, air enters the intake duct from the top of the fuselage and is then turned rearwards towards the fan. Design of this type of intake is simpler, since effectively only one turn of the flow is required once it has entered the duct. This layout however requires the fan drive shaft to extend from the fan across the intake duct (Figure 4), inevitably resulting in some disruption of the intake flow.

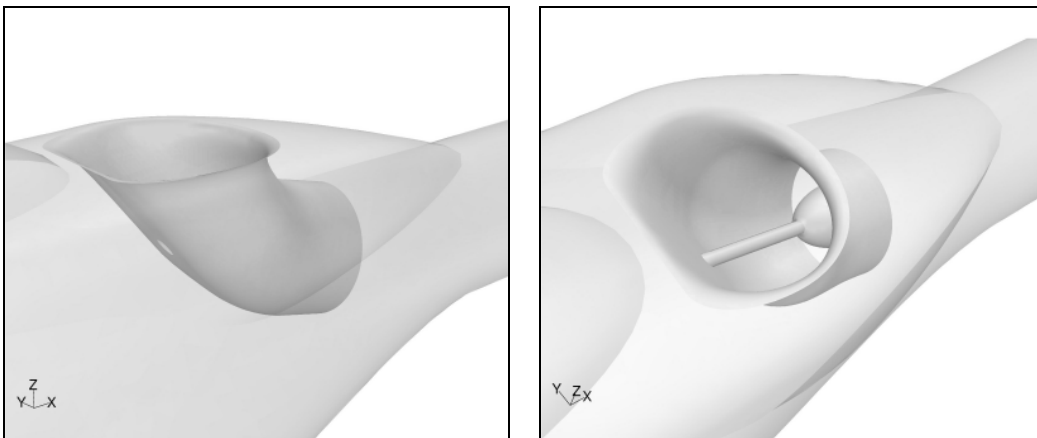


Figure 4 Top intake duct (fuselage displayed semi-transparent)

Design features of the top intake include the following:

- Entry area of the intake is on top of the fuselage, facing upwards for ideal capture of the rotor downdraft.
- Intake located behind gearbox cowling and between the two engines.
- Elliptical intake lips of large radius form the transition of fuselage into the duct.
- Duct entry centre line is slanted  $55^\circ$  upwards from the horizontal axis. The forward slant of the intake is to allow for an efficient capture of the air in forward flight.
- Intake flow is turned into the fan. The fan axis is tilted upwards by  $16.0^\circ$  from the horizontal axis.

- The shape of the capture area is derived from streamline patterns of a cross flow entering a hole on a flat plate, as described by Holdø et al<sup>(4)</sup>. The intake capture area is shaped to allow for a smooth inflow of the air from the stagnation zone behind the intake and saddle points on the side of the opening.

A similarly shaped cross section is used to describe the duct shape before transitioning to circular ahead of the fan. The intermediate cross section is elongated for better flow turning, as described by Sawyer<sup>(3)</sup>.

## 4 COMPUTATIONAL METHODS

### Grid Generation

The flow domain defined was 3.32 rotor diameters wide, extends 2.56 diameters upstream and 5.06 diameters downstream from the rotor centre. The domain was 2.21 diameters high, with the rotor origin located at two thirds height. For the low speed flights of  $\mu = 0.000$  and  $\mu = 0.015$  the domain was shortened downstream, but extended upwards by 0.5 diameters and downwards by 1.5 diameters. This is to prevent boundary condition effects and reduce recirculation of flow into the flow domain.

The mesh used was a combination of hexahedral and tetrahedral mesh elements, generated with the commercial code GAMBIT. The mesh for the rotor disk and hub was constructed from hexahedral cell elements, while the rest of the domain was constructed with tetrahedral elements. Use was made of the unstructured mesh for a finer resolution near the fuselage. The boundary layer mesh was constructed from prismatic elements, with a surface length of 82mm. The first element height of the boundary layer mesh was 0.1mm, with a growth rate of 1.6 for the following 8 elements. In the immediate vicinity of the fuselage the volume mesh size was 192mm, increasing to 300mm. For the far field elements the size increased to 1375mm.

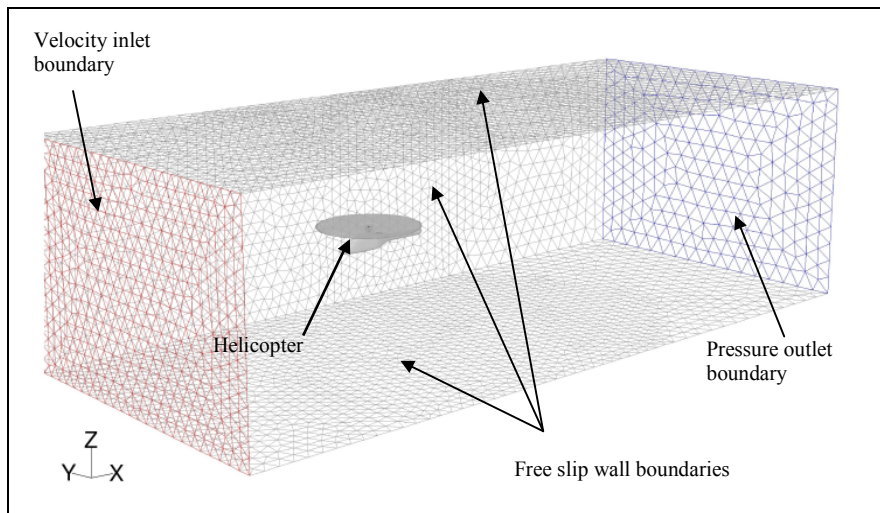


Figure 5 General mesh configuration

## Actuator Disk

For the CFD simulations the main rotor was modelled as an actuator disk. The actuator disk for the rotor included a model for the hub, to introduce the distorted flow resulting from the wake of the blade roots and control rods that make up the hub. In general the presence of the hub is often neglected in similar simulations; it is reasoned that the presence of the rotor hub can have a noticeable effect on the aerodynamics in and around the intakes, particularly due to the proximity of the intakes to the rotor hub.

The actuator disk model used utilises an upstream and downstream referencing method to calculate the blade section angle of attack. Air approaching an airfoil experiences an up wash ahead of the airfoil, and thus the section angle of attack must be measured upstream of the airfoil section. Thus for the actuator disk the section angle of attack must be picked up a small distance upstream of the actuator disk itself. This was first demonstrated by Meyer et al<sup>(5)</sup> and Hotchkiss et al<sup>(6)</sup>, while the concept was demonstrated by Heise et al<sup>(7)</sup> for use on helicopter rotor simulations. NACA 0012 profile data was used for the rotor blades, while for the actuator disk modelling the hub, lift and drag properties of a cylinder ( $C_L = 0.0$ ;  $C_D = 1.2$ ) were defined as the section properties. Balancing of the rotor for zero pitching and rolling moments around the hub was done on an iterative basis, with the assumption that the response to the pitching coefficients is linear.

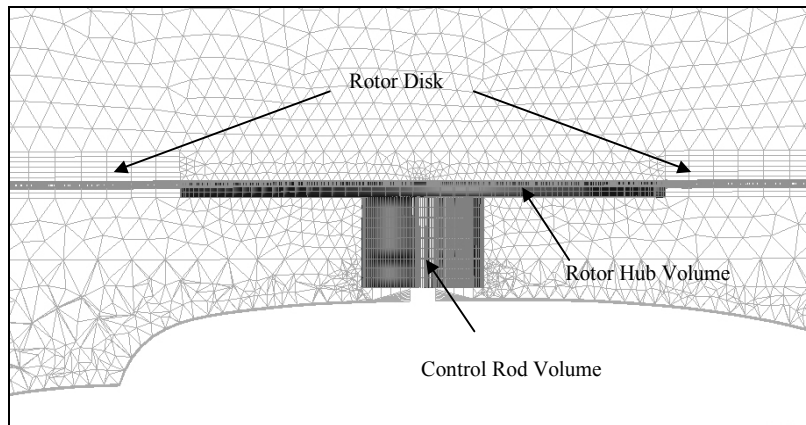


Figure 6 Schematic of the rotor and hub mesh configuration

The commercial CFD solver Fluent was used to resolve the flow in the domain, using an implicit formulation to solve the Navier-Stokes equations on the hybrid mesh. The flow equations are solved using a second order discretization scheme with a SIMPLEC pressure-velocity coupling algorithm. The steady, viscid and incompressible computations took between 700 and 1500 iterations to converge, depending on the case simulated. Due to the flow recirculation through the domain boundaries during the hovering and slow speed flight simulations, the computations took more than double the number of iterations to converge than the high-speed flight simulations.

## 5 COMPUTATIONAL RESULTS

The analysis of the intakes presented here follows the traditional way of analysing the performance of intakes by focusing on parameters such as efficiency, duct loss and distortion at the fan face. Here however an additional parameter is investigated, namely that of the average pressure coefficient on the capture plane of the intake. These figures are thus essentially a measure the effectiveness of the location of the intake opening on the fuselage.

To calculate the pressure coefficient of the intake capture plane, the average pressure on the capture plane is taken from the CFD results and normalised with the dynamic pressure of the flow through the rotor, as shown in Equation 1. In the presentation of the data here, the figures are normalised by the average velocity through the rotor disk, as calculated by momentum theory (Seddon<sup>(8)</sup>). The use of this velocity, instead of the usual free stream velocity, avoids the division by zero at  $\mu = 0.00$  in the definition of the pressure coefficients. Additionally it provides a better measure for normalisation of the intake performance parameters, as the intakes are significantly affected by the rotor downwash.

$$C_p = \frac{P_C - P_\infty}{q_{MR}} \quad (1)$$

The intake efficiency is defined as the average total pressure over the entire fan face divided by the rotor disk dynamic pressure, as in Equation 2.

$$\eta = \frac{P_f - P_\infty}{q_{MR}} \quad (2)$$

Intake duct losses are defined as the average total pressure loss of the air inside the intake duct, normalised with the dynamic pressure at the fan face, as in Equation 3. This gives a measure of the effectiveness of the intake duct, and thus of the design of the intake.

$$\text{Duct Loss : } C_{\Delta P} = \frac{\Delta P_d}{q_f} \quad (3)$$

The final parameter through which the intake designs are analysed is the total pressure distortion on the fan face. The most commonly used distortion coefficient is the DC60 coefficient; this factor describes the fan face distortion by subtracting the mean total pressure of a  $60^\circ$  sector with the lowest mean total pressure from the average total pressure over the entire face and then dividing that result by the mean dynamic pressure over the face (Cumpsty<sup>(9)</sup>), as shown in Equation 4.

$$DC(\theta) = \frac{P_f - P_\theta}{q_f}; \theta = 60^\circ \quad (4)$$

### Side Intakes

Results discussed in this section are for the side intakes of the single engine helicopter for the three contraction ratios over the selected range of advance ratios. Comparison

is also made of the effects of the inclusion of the rotor hub in the computations has on the performance of the intakes. The rotor flow conditions, as calculated by momentum theory, used in the calculation of the coefficients for the single engine helicopter are given in Table 1.

Table 1 Rotor and flow specifications used for the side intake evaluation

	$C_T = 0.00555$	$R = 5.5$ [m]	$RPM = 350$	# Rotor Blades = 3	
$\mu$	0.000	0.015	0.050	0.149	0.198
$V_{MR}$	10.62	10.83	13.21	30.27	40.01

### 5.1.1 Capture Area Pressure Coefficient

Figure 7 shows the average total pressure coefficients at the capture plane of the side intakes over the range of tested advance ratios. At  $\mu = 0.00$  there is only a small difference between the hub and the no-hub results: the hub results have a slightly higher value of about  $C_p \approx 0.1$  for all contraction ratios. The hub thus has a small positive influence here. The contraction ratio however has a noticeable effect at low advance ratios; a higher contraction ratio, and thus a larger net capture area, gives a better performance.

At  $\mu = 0.015$  the hub included results are decidedly worse, indicating a strong influence of the hub at this advance ratio. As can be seen by the streamlines entering the intake in Figure 11 the flow first passes through the hub, and is thus subjected to significant losses. Increasing the contraction ratio again helps, but not significantly above a contraction ratio of  $CR = 3.0$ .

For advance ratios higher than  $\mu = 0.050$  the difference between the hub and no-hub results becomes smaller because the hub wake is now convected past the inlet area. Above  $\mu = 0.050$  the relative influence of the contraction ratio also becomes smaller.

At  $\mu = 0.050$  the  $C_p$  value is larger than one due to the majority of the flow entering the intake no longer being subjected to the losses of the hub at this advance ratio. Instead that flow passes through the rotor blades and work is done on the flow, increasing its total pressure from the free stream conditions. The non-uniform load distribution on the rotor causes some of the flow to gain a higher total pressure when compared to the disk average, which thus can result in a pressure coefficient above unity due to the average disk dynamic pressure being used to calculate the coefficient. For this specific case the total pressure at the intake entry plane exceeds the average due to the captured flow first passing through a highly loaded sector of the rotor, resulting in the  $C_p$  higher than unity.

### 5.1.2 Intake Efficiency

An overall intake efficiency is presented in Figure 8, with the efficiency defined as per Equation 2. There is a distinct difference visible in the intake efficiencies for the different contraction ratios, the higher contraction ratios giving better efficiency values. Also noticeable is the relatively small advantage of the  $CR = 3.5$  over the  $CR = 3.0$  intake when compared to the  $CR = 2.5$  intake. The effect of the rotor hub is

small for respective contraction ratios, similar as discussed in section 5.1.1, with the influence on the efficiency being negligible above  $\mu = 0.05$ .

### 5.1.3 Duct Losses

Figure 9 shows the duct losses of the side intakes, and the effect the contraction ratio has on the duct losses is immediately apparent. The two higher contraction ratios show significantly lower losses over the entire range of advance ratios, with up to 30% lower losses. Again the difference between CR = 3.0 and CR = 3.5 is not as significant as that between CR = 2.5 and CR = 3.5. The relative influence of the rotor hub on the duct losses is small; it slightly improving the performance at  $\mu = 0.00$ , with the trend reversing at  $\mu = 0.015$ . No difference is detected at higher advance ratios.

### 5.1.4 Distortion

At hover the fan face distortion from the side intakes is mildly sensitive to contraction ratio (Figure 10), but again not much difference evident above CR = 3.0, with the lowest distortion being DC60 = 0.04. At the low advance ratios of  $\mu = 0.00$ , and specifically at  $\mu = 0.015$ , the inclusion of the hub has a significant influence; the distortion is lower with the hub included at  $\mu = 0.00$ , but higher again at  $\mu = 0.015$ . At  $\mu = 0.015$  the rotor hub creates a helical flow pattern (also visible in Figure 11), predominantly on the advancing side, that gets ingested by the intake on that side and thus causes the higher distortion. For advance ratios above  $\mu = 0.05$  the hub has little of no effect on the distortion, as its wake is then convected past the intakes.

Contours of total pressure distribution at the fan face for the five advance ratios are shown in Figure 12, looking at the fan face in the downstream direction (Note the different scale for each plot). The plots are for the CR = 3.0 side intake with rotor hub included only, but show the trends in distortion patterns that are evident for all contraction ratios. At hover,  $\mu = 0.000$ , there are two low pressure cells at the 3 and 9 o'clock position. As the flight speed advances to a low speed of  $\mu = 0.015$ , the swirl in the rotor wake entering the intake causes the low pressure cells to migrate to the 2 and 8 o'clock positions respectively. At  $\mu = 0.050$ , where the rotor wake is already convected past the inlets, the cells return to the original positions while at the same time reducing in strength. Distortion values then pick up again at  $\mu = 0.149$  to  $\mu = 0.198$ , due to separation of the lower intake lips.

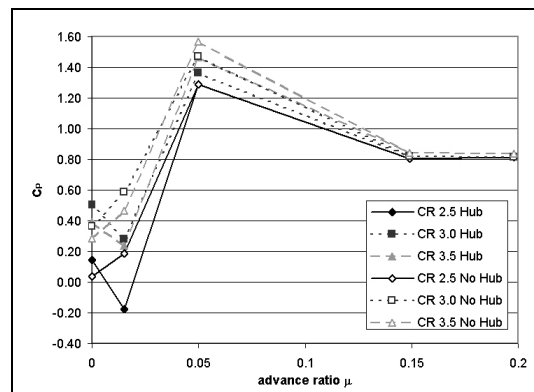


Figure 7 Capture plane total pressure coefficients, side intakes

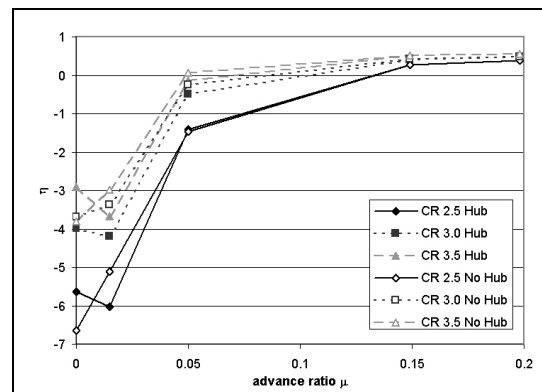


Figure 8 Intake efficiency, side intakes

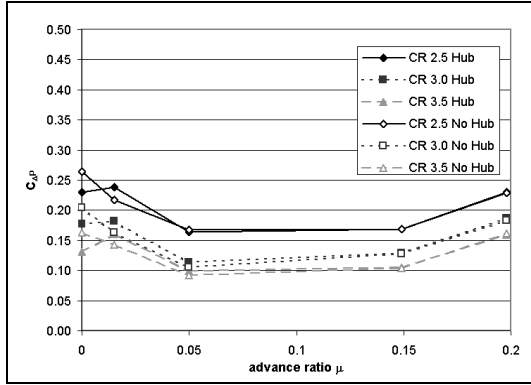


Figure 9 Duct loss, side intake

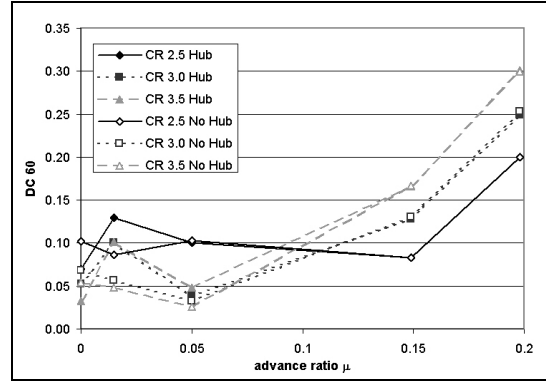


Figure 10 Fan face distortion values, side intakes

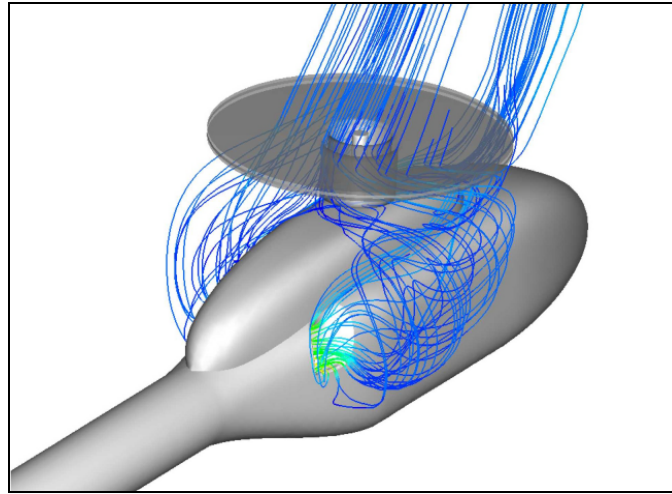


Figure 11 Streamlines entering the intakes at  $\mu = 0.015$

## Top Intakes

The alternative design of the top mounted intake for the twin helicopter was also evaluated for the three contraction ratios and the same five advance ratios. A comparison is also again made between results that include and exclude the rotor hub in the numerical solutions. The rotor flow conditions, as calculated by momentum theory, used in the calculation of the coefficients for the single engine helicopter are given in Table 2.

Table 2 Rotor and flow specifications used for the top intake evaluations

	$C_T = 0.00668$ $R = 5.5$ [m] $RPM = 384$ # Rotor Blades = 4				
$\mu$	0.000	0.015	0.050	0.149	0.198
$V_{MR}$	12.78	13.00	15.35	33.32	43.95

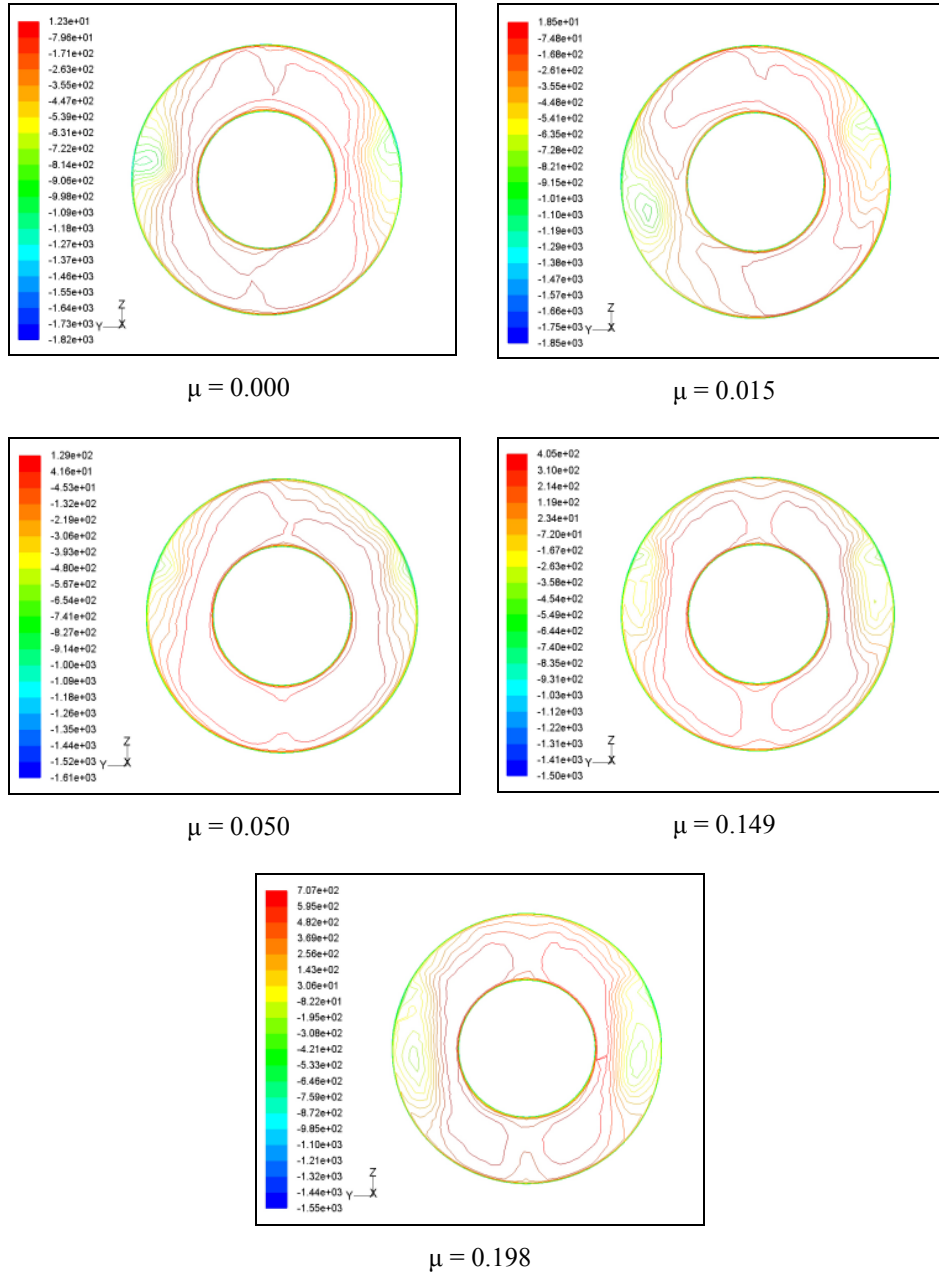


Figure 12 Fan face total pressure contours of the side intakes (CR = 3.0)

### 5.1.5 Capture Area Pressure Coefficient

The  $C_p$  values in Figure 13 present the average intake capture plane total pressure coefficient for the top opening intake, as defined in Equation 1. At  $\mu = 0.00$  the effect of the inclusion of the rotor hub is small; the hub only slightly reducing the total pressure available to the intake by a maximum of  $C_p \approx 0.1$ . For the conditions at  $\mu = 0.015$  most of the flow entering the intake first passes through the rotor hub and is thus subjected to the drag losses of the rotor hub. See also Figure 17 for the stream lines entering the intake. At  $\mu = 0.015$  (Figure 13) the CR = 3.5 intake shows a significant advantage above the other contraction ratios with a  $C_p = 0.21$  versus  $C_p \approx 0$  of the other intakes that include the hub. For the cases where the hub was not

included there is no significant drop in the available total pressure at the entry plane from hovering conditions.

At  $\mu = 0.05$  the flow entering the intake is still strongly affected by the rotor hub and the flow patterns it creates. But the flow itself does not pass through the hub volume first and hence the losses are less than at  $\mu = 0.015$ , as can be seen by the  $C_p$  values of  $C_p \approx 0.45$ .

The  $C_p$  values for the no-hub case are again above unity at  $\mu = 0.05$ , for the same reasons already explained with the side intakes. Apparent at  $\mu = 0.05$  is also the effect the hub has on the intake; there is a difference of  $C_p \approx 0.6$  between the hub on and off cases, indicating the strong losses the rotor hub incurs on the intake at this advance ratio. At the higher advance ratios above  $\mu = 0.05$  the hub does not have a dominating influence anymore, a difference of  $C_p \approx 0.1$  being predicted.

### **5.1.6 Intake Efficiency**

Using the definition of intake efficiency of Equation 2, the overall intake efficiency for the top intake is shown in Figure 14. Unlike the side intakes, the rotor hub has a distinct effect on the efficiency of the intakes. The effect is small at low speed flight, but a dominating influence is shown at the advance ratio  $\mu = 0.05$ , with the difference contributed by the hub being about 1.5 efficiency points for all contraction ratios. Increasing the contraction ratio has a significantly positive effect on the efficiency performance of the intake, but again not much is to be gained from a higher contraction ratio than 3.0.

### **5.1.7 Duct Loss**

In Figure 15 the average duct loss of the top intake is shown; again normalised with the average dynamic pressure on the fan face, as described by Equation 3

Evident is again the effect an increasing contraction ratio has on the losses of the duct, with the relative improvement of a contraction ratio above 3.0 being small. At hover the duct loss difference between  $CR = 2.5$  and  $CR = 3.0$  is roughly 0.07, with the remainder of the results varying  $C_{\Delta P} \approx 0.01$  from each other. For the higher contraction ratios the losses also remain relatively constant around 0.08. A difference of the hub and no-hub results can be seen at  $\mu = 0.05$ , as this is the advance ratio where the hub wake has the most significant effect on the intake. Similar duct losses for all intakes at high advance ratios indicate a low dependence on contraction ratios.

### **5.1.8 Distortion**

The distortion for the top intake is distinctly sensitive to the contraction ratio, as can be seen from Figure 16. The larger contraction ratios give lower distortion values at the low advance ratio end of the flight envelope, though the trend reverses at  $\mu = 0.149$ , where the  $CR = 2.5$  intake shows slightly better results. Similar to the same trend already identified, there is no drastic difference between the contraction ratios of  $CR = 3.0$  and  $CR = 3.5$ . Interesting to note is that the inclusion of the hub improves the DC60 values notably at  $\mu = 0.015$  for all contraction ratios. The trend is however reversed dramatically at  $\mu = 0.050$ .

The reason for the low DC60 values at  $\mu = 0.015$  is as a result of the rotor hub feeding air into the intake from the retreating side (this does not happen in the no-hub case), and little of the swirling flow on the advancing side is ingested; this resulting in a

better flow quality at the fan face. The reversal in the trend follows from a change of the side from which air gets inducted; between  $\mu = 0.015$  and  $\mu = 0.050$  the incoming intake flow switches from the retreating to the advancing side of the fuselage. The flow patterns that are formed by the hub on the advancing side (Figure 18) now get ingested into the intake in full and influence the fan distortion negatively.

Contours of total pressure at the fan face for the five advance ratios are shown in Figure 19, looking at the fan face in the downstream direction. (Note the different scale for each plot). The plots are for the CR = 3.0 top intake with rotor hub included only, but show the trends in distortion patterns that are evident for all contraction ratios. At hover,  $\mu = 0.00$ , there is a single low pressure cell at the 12 o'clock position which is as a result of separation inside the duct bend. As the flight speed increases to a low speed ( $\mu = 0.015$ ) another low pressure region appears at the 7 o'clock position due to the fan shaft wake. Swirl from the rotor wake causes a slight anti-clockwise shift of the low pressure regions at  $\mu = 0.05$ . At  $\mu = 0.149$ , where the rotor wake influence is small on the inlets, symmetry of the pressure contours is restored. Distortion values then pick up again slightly at  $\mu = 0.198$ , a result of cowling wake and the effects of the intake operating at a high incidence.

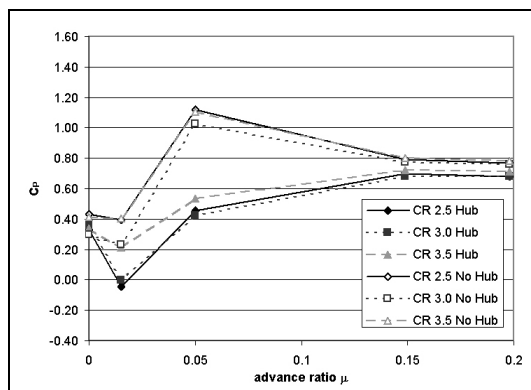


Figure 13 Capture area total pressure coefficients, top intake

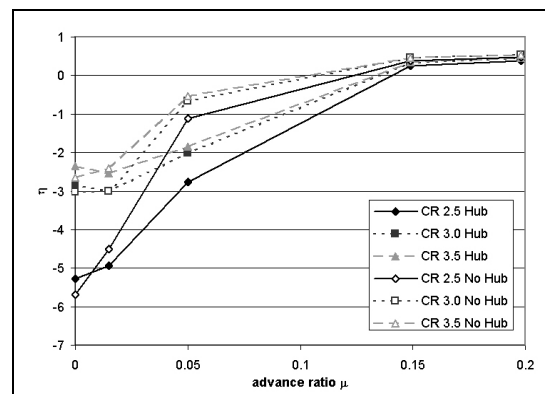


Figure 14 Intake efficiency, top intake

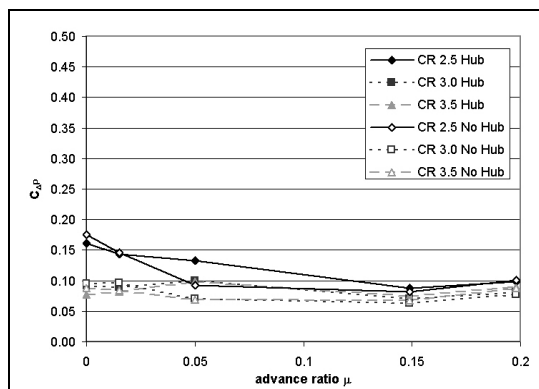


Figure 15 Duct loss, top intake

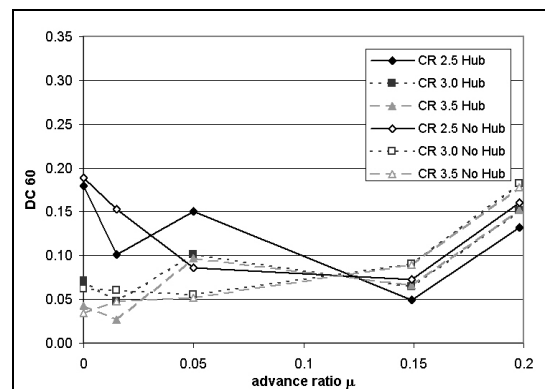


Figure 16 Fan face distortion values, top intake

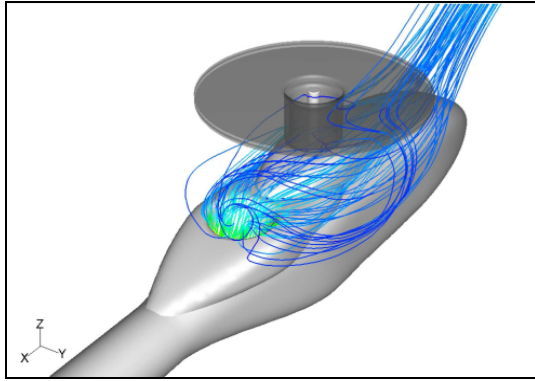


Figure 17 Streamlines entering the top intakes at  $\mu = 0.015$

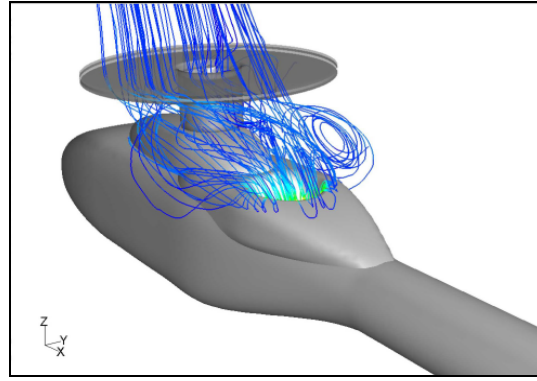


Figure 18 Streamlines entering the intake, predominantly from the advancing side, at  $\mu = 0.050$

### Comparison of Side Mounted to Top Mounted Intakes

Here a side-by-side comparison of the two intake concepts is presented to give a better indication of the relative advantages each concept presents. Results used here for the comparison are only from the rotor hub inclusive cases, but for all three contraction ratios. The comparisons are made according to the same parameters used for discussion in the previous sections on the individual designs.

#### 5.1.9 Capture Area Pressure Coefficient

Looking at the average total pressure available for each concept at the intake capture plane makes a beneficial direct comparison between the two concepts. Here any sub-optimal designs of the duct itself are excluded, allowing for analysis of the design specific issues that need to be considered for the location of the intake. The  $C_p$  values in Figure 20 are again normalised with the rotor dynamic pressure as per Equation 1

At hover the average total pressure at the capture plane of both intakes is virtually the same, except for the  $CR = 2.5$  and  $CR = 3.0$  side intakes that show a slight variation. Consequently no preferred location of the intake opening at hover can thus be established, as long as a contraction ratio of at least 3.0 is used.

For  $\mu = 0.015$  the rotor hub influences both designs negatively, more so for the top intake. But as can be seen in Figure 20 a larger capture area (and resultantly bigger contraction ratio) helps to improve the top intake performance.

In the intermediate speed range of  $\mu = 0.050$  the side intakes have a clear advantage. Here the hub wake is already convected past the side intakes, while the top intake still inducts air that is strongly affected by the hub. At the high flight speeds the total pressure available to the intakes is similar, however the top intake is now located in the wake of the gearbox cowling and thus has a slight pressure deficiency.

#### 5.1.10 Intake Efficiency

With regard to the intake efficiency at hover the position does not have a big influence (Figure 21), with the top intake faring only slightly better. More significant is the contraction ratio to obtain a better performance. This is also true for the intake performances around  $\mu = 0.015$ . In the mid speed range the initial total pressure

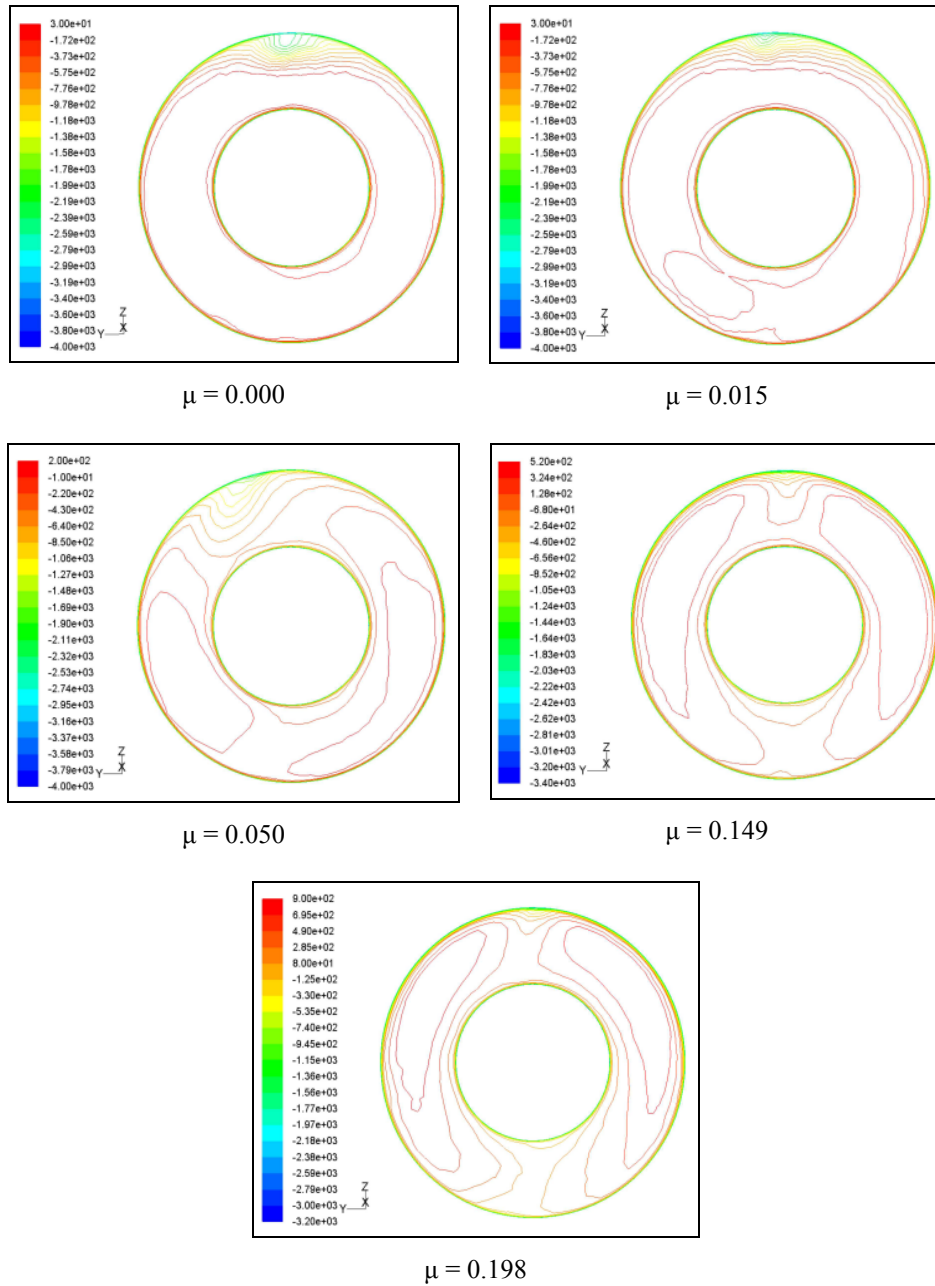


Figure 19 Fan face total pressure contours of the top intake (CR = 3.0)

deficiency (Figure 13) of the top intake causes a lower overall efficiency compared to the side intakes, until at higher speeds the efficiency values are again the same. The efficiency is however also dependent on the losses in the intake duct, which are discussed next.

### 5.1.11 Duct Loss

Comparing the duct losses of Figure 22 for the two concepts, it is clear that the top intakes perform noticeably better at low speeds, especially the two intakes featuring the higher contraction ratios. This is primarily as a result of the simpler/cleaner duct shape possible with the top intake, while on the other hand the side intakes require a series of complex three-dimensional S-bend turns in a confined volume. These rapid

changes in the duct cause losses which are evident by the high losses of up to  $C_{\Delta P} = 0.25$  for low flight speeds. Here a large contraction ratio helps to bring the losses under control. The two higher contraction ratio top intakes show an almost constant  $C_{\Delta P}$  not exceeding  $C_{\Delta P} = 0.1$  for the entire range of flight speeds. It can be noted here that for a straight duct of similar size to the intake duct, the pressure drop is  $C_{\Delta P} = 0.45$ , which is close to half of that displayed here. At higher speeds the duct losses increase as a result of the intakes now operating at a high incidence.

### 5.1.12 Distortion

With a relative comparison of the DC60 factors (Figure 23) for the two concepts there is no clear advantage. For the entire fan face most of the designs have a similar distortion value of about  $DC_{60} = 0.04$  to  $DC_{60} = 0.06$ , except the CR = 2.5 top intake. As the flight speed increases, the rotor hub negatively influences the side intakes; the DC60 value increases to almost double the value at hover. The trend is reversed at  $\mu = 0.050$  where the top intakes takes the brunt of the hub wake. Beyond  $\mu = 0.050$  there is a gradual increase of the DC60 factors for all intakes as they start to operate at progressively higher angles of incidence. The comparatively higher DC60 values of the side intake are partly as a result of the intake shaping that is optimised to work at low advance ratios.

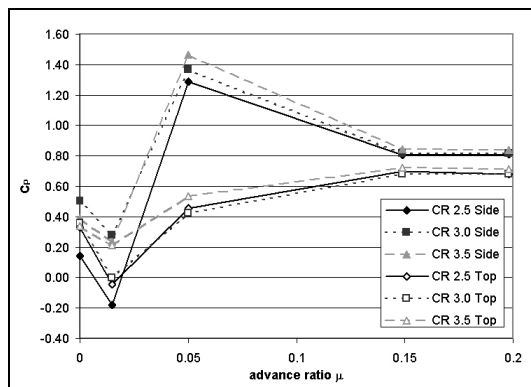


Figure 20 Capture area total pressure coefficients

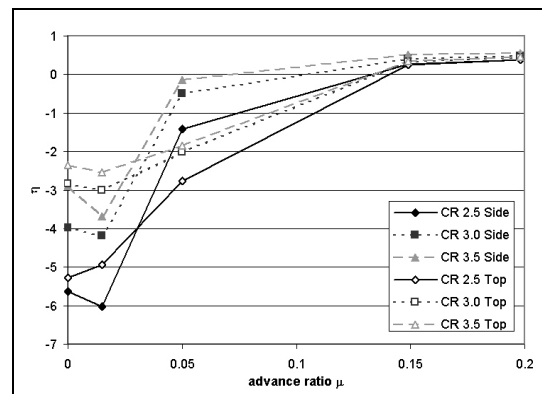


Figure 21 Intake efficiencies

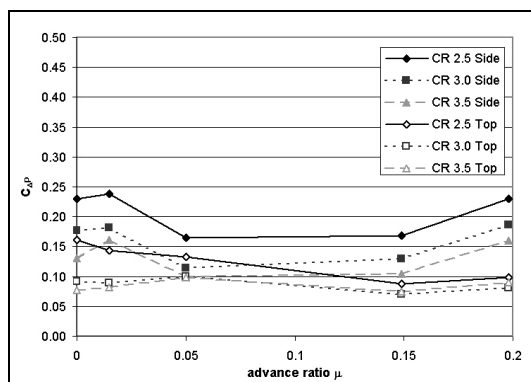


Figure 22 Duct losses

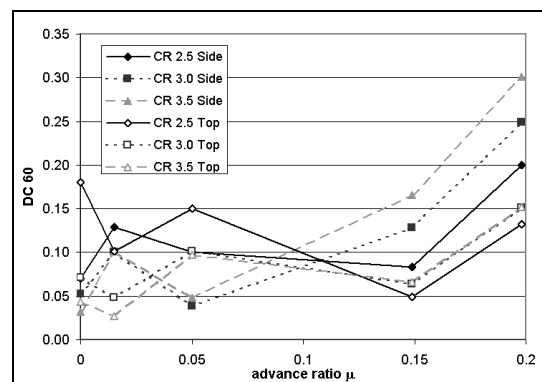


Figure 23 Fan face distortion values

## Conclusion

The objective of the intake evaluation was to analyse two intake concepts for the two-stream fan on a generic fuselage configuration. The studies concentrated on the evaluation of design parameters such as intake location, contraction ratio and the role the rotor and its hub have on intake performances.

Initially it was hoped that positioning the intake on top of the fuselage would allow it to capture the rotor downwash, and thus have flow of a higher total pressure enter the intake. This did not prove to be the case. This can firstly be attributed to the reduced downwash velocity near the centre of the rotor, compared to the average of the rotor disk, and secondly to the losses the rotor hub adds to the flow entering the intake. In this respect the advantage of the top over the side intakes intake in hovering conditions is therefore small. Another point of consideration for the top intake is the wake of the gearbox cowling and rotor hub that constantly affect the intake, specifically between  $\mu = 0.05$  to  $0.15$  in the current configuration.

A factor that affects both intakes is the switch of side of the incoming intake flow, particularly at low speed. At advance ratios below  $\mu = 0.015$  the flow gets induced predominantly from the retreating side after which it changes to the advancing side.

Controlling duct losses has been shown to be more difficult with the side mounted intakes, due to the intricate duct shape. Increasing the contraction ratio proves to be an effective method to control the losses, as well as to limit the distortion on the fan face. Through all investigated performance parameters the trend was consistent, namely that increasing the contraction ratio above 3.0 does not yield significant performance improvements.

The rotor hub has a predominantly performance degrading effect on the intakes. The rotor hub adds losses to the incoming flow while at the same time creating a flow pattern that causes a higher distortion at the fan face, particularly during the slow flight phase. It is thus important to model the hub with any performance evaluations of the intakes.

In general there is no distinct advantage to either intake. Below advance ratios of about  $\mu = 0.03$  the top intake does appear to be the better choice due to its higher overall efficiency, lower losses and low distortion coefficients for the entire fan face. A reversal of these advantages then occurs between  $\mu = 0.03$  and  $\mu = 0.150$  where the side intakes have the advantage due to the hub wake already being convected past the intake openings.

At the high speed end of the flight envelope the side intakes suffer from high distortion levels due to the design being optimised for low speed flight and by the addition the scoop on the lower sector of the inlet opening. This scoop and the effectively high angle of attack experienced by the intake at high advance ratios cause some separation at the duct entrance resulting in the pressure and flow distortion. Additionally the flow entering the side intakes (streamlines shown in Figure 24) first flows along the side of the fuselage and is thus subject to the losses in the fuselage boundary layer.

The top intake design does not display these characteristics to the same extent even though it is also operating at high angles of attack at this high speed stage of the flight envelope. By placing the intake on top of the fuselage less turning of the incoming

flow is required, while at the same time less of the flow entering the intake is affected by the fuselage/cowling boundary layer. It also appears that the presence of the gearbox cowling reduces the local angle of attack as some of the flow is already turned downwards toward the intake by the cowling as can be seen by studying the streamlines shown in Figure 25.

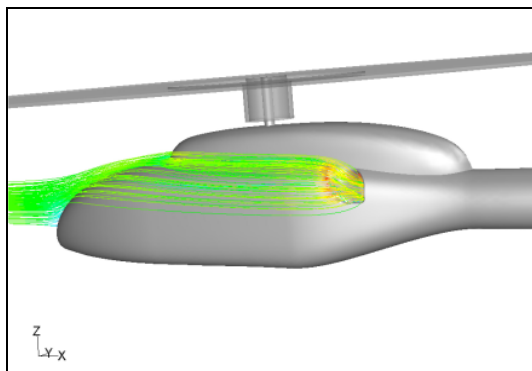


Figure 24 Streamlines entering the side intakes at  $\mu = 0.198$

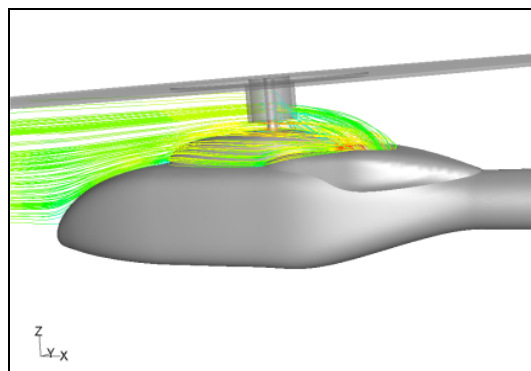


Figure 25 Streamlines entering the top intake at  $\mu = 0.198$

As a general design guideline it is suggested here to design these intakes with a specific focus on hovering conditions. The current intakes were designed as a compromise between hover and high speed flight by angling the entrance of the intake duct forward by up to  $35^\circ$ . This resulted in the reduced performance shown at low and high end of the advance ratios and an increase in the DC60 coefficients with increasing advance ratio. In the mid speed range, where the relative angle of attack of the intakes is low, both intake versions show good performances. Use should thus rather be made of the increased dynamic pressure of the incoming flow at higher advance ratios to offset the reduced intake performance.

## 6 REFERENCES

- [1] Mineck, R.E., Althoff Gorton, S., (2000), *Steady and Periodic Pressure Measurements on a Generic Helicopter Fuselage Model in the Presence of a Rotor*, NASA TM 2000-210286.
- [2] Seddon, J., Goldsmith, E.L. (1999), *Intake Aerodynamics*, Second Edition, Blackwell Science.
- [3] Sawyer, J.W. (1976), *Sawyer's Gas Turbine Engineering Handbook, Vol. 1*, Second Edition, Gas Turbine Publications, Inc. 80 Lincoln Ave., Stanford, Connecticut, 06904.
- [4] Holdø, A.E., O'Brien, M., Calay, R.K., (2000), *Flows Generated by the Interaction of an Inlet and a Cross-Flow*, Journal of Wind Engineering and Industrial Aerodynamics, Vol. 88 (2000), pp. 1-23.
- [5] Meyer, C.J., Kröger, D.G., (2002), *Numerical Simulation of the Flow Field in the Vicinity of an Axial Flow Fan*, International Journal of Numerical Methods in Fluids.

- [6] Hotchkiss, P.J., Meyer, C.J., von Backström T.W. (2006), *Numerical Investigation into the Effect of Cross-Flow on the Performance of Axial Flow Fans in Forced Draught Air-Cooled Heat Exchangers*. *Applied Thermal Engineering* 26 (2006), pp 200-208.
- [7] Heise, R. (2005), *Development of a Method for CFD evaluation of Helicopter Fuselages*, Paper No. 12, 31<sup>st</sup> European Rotorcraft Forum, Florence, Italy, September 2005
- [8] Seddon, J. (1990), *Basic Helicopter Aerodynamics*, AIAA /Blackwell Science.
- [9] Cumpsty, N.A. (1989), *Compressor Aerodynamics*, Longman Scientific & Technical, Essex, UK.